Investigation of Polyethylene by Means of Magic Angle Turning and Separated-Local-Field Experiments

Jian Zhi Hu,[†] Wei Wang,[†,⊥] Shi Bai,[†,#] R. J. Pugmire,[*,‡] Craig M. V. Taylor,[§] and D. M. Grant[*,†]

Departments of Chemistry and Chemical and Fuels Engineering, University of Utah, Salt Lake City, Utah 84112, and Los Alamos National Laboratory, Los Alamos, New Mexico 87545

Received October 6, 1999

ABSTRACT: The principal values of the ^{13}C chemical shift tensors and the $^{1}H-^{13}C$ separated-local-field patterns are reported for the all-trans structures with long and short T_1 as well as the more and less mobile amorphous segments in polyethylene. It is shown that the principal values of the chemical shift tensor, and the local ^{1}H field of the tensor, for the all-trans crystalline structures with long and short T_1 are essentially the same, supporting the previous suggestion by Schmidt-Rohr and Spiess that chain diffusion between the amorphous and the crystalline regions in PE is the primary reason for the multiexponential ^{13}C T_1 relaxation observed for the all-trans peak observed at 33 ppm. The less mobile amorphous component adopts preferably a trans conformation and undergoes a fast rotation dominantly about the molecular axis at a rate larger than the width of the CH_2 group dipolar coupling. The motion involved in the mobile amorphous structure approaches isotropic tumbling, but a modest amount of constrained reorientation remains. Consequently, the $^{13}C-^{1}H$ dipolar coupling is averaged out, but the shift tensor is not totally averaged to its isotropic value.

1. Introduction

The dynamics and structures of polymers may be characterized at a molecular level by a variety of solid-state NMR techniques.[1] Because of its simple structure as well as its industrial importance, polyethylene (PE) has provided a model polymer system for many years. Three types of structures (i.e., crystalline, interfacial, and amorphous) with different motional properties were proposed initially on the basis of wide-line ^{1}H NMR work.[2−6] These structures have been corroborated by high-resolution ^{13}C MAS studies which are more sensitive to differences in chain conformation and dynamics.[7−11] It is generally accepted that the narrower resonance centered at about 33 ppm arises from the ordered crystalline carbons with an all-trans conformation while the broader resonance centered at approximately 31 ppm arises from the less ordered amorphous regions (or domains) consisting of gauche structures mixed into the trans conformations. As many as four different structural units have been proposed to interpret the ^{13}C spectra.[11]

By decomposing the ^{13}C CP/MAS spectra of PE into two resonances at 31 and 33 ppm, Cheng et al.[14] studied the ^{13}C T_1 relaxation in a series of high-density linear PE samples with different histories. It was clearly demonstrated that the ^{13}C T_1 relaxation for the resonance located at 33 ppm is double-exponential, with one relaxation time on the order of several hundred seconds, while the other is as short as 1−3 s. These authors assigned the long ^{13}C T_1 relaxation to crystalline carbons and the short ^{13}C T_1 component to the interfacial structures.[14]

Dipolar-dephasing, single-pulse ^{13}C MAS experiments[1,11] show that the broad line assigned to the amorphous region has a complex distribution of residual $^{13}C-^{1}H$ dipolar couplings. These data may be interpreted in terms of interfacial material with constrained motions and of near isotropic chain motion in CH_2 groups that are more remote from the crystalline domains.

Evidence of a magnetization transport mechanism between the amorphous and the crystalline carbons has been found in a 2D exchange experiment.[12,13] Physical diffusion of the chain between these two regions was suggested as the possible cause of the multiexponential ^{13}C T_1 behavior of the crystalline resonance signal at 33 ppm.

Though high-resolution ^{13}C MAS studies on PE have been very fruitful, there remains contradictions in the literature regarding the nature of the interfacial structures. Hence, the physical picture of the chain conformation and molecular motion in the interfacial structure (which is designated as a less mobile amorphous structure in this work) needs further clarification.

It is well-known that the principal values of the ^{13}C chemical shift tensor, which provides three times more information than the isotropic chemical shift, are lost in a MAS experiment when the spinning rate exceeds the width of the shift tensor. Furthermore, the $^{13}C-^{1}H$ dipolar coupling tensor, which is sensitive to molecular motion, is also lost in a high-speed MAS experiment along with useful information on the orientation of the shift tensor.

In the present work we have utilized multiple component ^{13}C T_1 data to explore the shift tensor principal values. The large differences in the values of ^{13}C T_1 and in the dipolar dephasing time constants provides a basis in the 2D magic angle turning (MAT) experiments[16−19] to selectively measure the principal values of the crystalline, less mobile amorphous, and the mobile amorphous structures in PE. The local ^{1}H dipolar field at the

[†] Department of Chemistry, University of Utah.
[‡] Department of Chemical and Fuels Engineering.
[§] Los Alamos National Laboratory.
[⊥] Present address: Department of Chemistry, Princeton University, Princeton, NJ 08544.
[#] Present address: Department of Chemistry and Biochemistry, University of Delaware, Newark, DE 19716.

10.1021/ma9916842 CCC: $19.00
Published on Web 05/02/2000

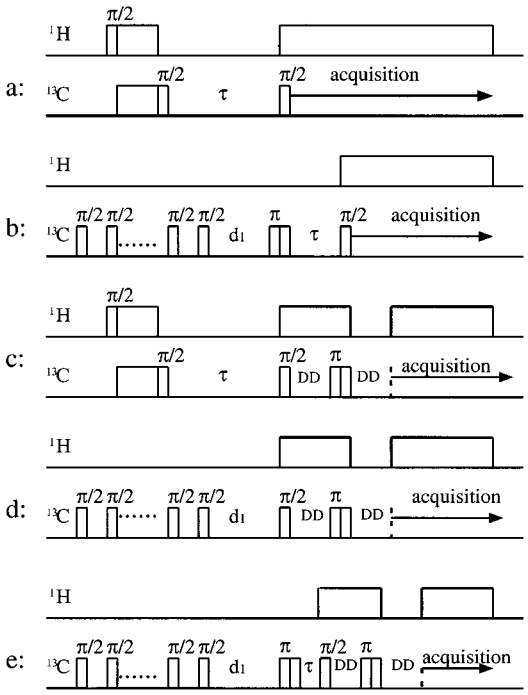

Figure 1. Pulse sequences for the measurement of ^{13}C T_1 values and for determining the dipolar dephasing constants for the different structures in PE. (a) The conventional inversion−recovery method via CP. (b) Inversion−recovery combined with saturation−recovery. (c) Dipolar dephasing combined with CP−inversion−recovery. (d) Dipolar dephasing combined with saturation−recovery. (e) Dipolar dephasing combined with saturation−recovery plus inversion−recovery.

^{13}C nucleus for the crystalline, less mobile amorphous, and mobile amorphous carbons in PE were measured with the 2D separated-local-field experiment.[20] Such 2D experiments produce additional spectroscopic information that provides new insights into the microscopic molecular structure and morphology of polyethylene.

2. Experimental Results

2.1. ^{13}C T_1 and Dipolar Dephasing Results. The polyethylene (PE) sample investigated in this work was Phillips EHM-6003 with $M_w = 145\,000$, $M_w/M_n = 7.8$, density = 0.962 g/cm^3, and a melting temperature of 136 °C measured by DSC.

The high-resolution ^{13}C MAS, ^{13}C T_1, and the ^{13}C−^{1}H 2D separated-local-field experiments on this sample were carried out on a Chemagnetics CMX-400 NMR spectrometer with a ^{13}C Larmor frequency of 100.6 MHz. A Chemagnetics MAS probe with a 7.5 mm (o.d.) sample rotor was used. Both the cross-polarization and ^{1}H decoupling fields were 67.6 kHz.

The pulse sequences for the selective measurement of ^{13}C T_1 values for the all-trans structures with both long and short ^{13}C T_1 values as well as the amorphous structures are summarized in Figure 1a,b. The pulse sequences for determining the dipolar-dephasing constants for the various types of structures in PE are given in Figure 1c−e.

A typical ^{13}C CP/MAS spectrum of PE obtained at a 4 kHz spinning speed is shown in Figure 2a. The ^{13}C spin−lattice relaxation time (T_1) can be measured using the indirect CP sequence shown in Figure 1a. As reported by Kitamaru et al.,[11] the recovery of the magnetization of the 33 ppm peak requires a multiexponential fit with three times of 1010 s (61%), 93 s (26%), and 2.1 s (13%). This analysis of crystalline peak at 33 ppm probably is comparable to a continuous distribution of ^{13}C T_1. A T_1 value of approximately 0.3 s was obtained for the amorphous peak centered at 31 ppm. A transient NOE effect, which can be further suppressed by using the phase cycling proposed by Torchia,[15] is also observed for the amorphous peak when the traditional inversion−recovery is used.

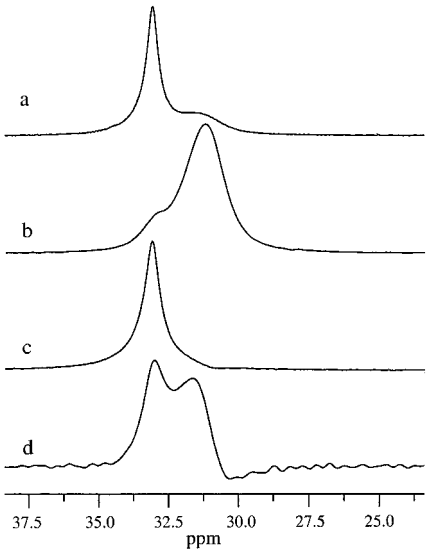

Figure 2. (a) Standard ^{13}C CP/MAS spectrum of PE. (b) The spectrum, phase inverted, was obtained with the pulse sequence in Figure 1b using parameters $d_1 = 0.4$ s and recovery time $\tau = 1$ μs. (c) The spectrum, phase inverted, was obtained using the pulse sequence in Figure 1c with DD = 0 μs and a recovery time of $\tau = 0.3$ s. (d) The spectrum, phase inverted, was obtained with the pulse sequence in Figure 1e using parameters $d_1 = 0.4$ s, recovery time $\tau = 0.135$ s, and a dipolar dephasing period of $\tau = 0$ μs.

To measure accurately the ^{13}C T_1 values of the amorphous structures at 31 ppm and the short ^{13}C T_1 value peak at 33 ppm, the selective pulse sequence in Figure 1b was employed, in which the 1010 and 93 s ^{13}C T_1 relaxations were saturated with a train of $\pi/2$ pulses separated by about 200 μs. The representative spectra with inverted phases were acquired using parameters $d_1 = 0.4$ s, and recovery times $\tau = 1$ μs and 0.135 s are depicted in parst b and d of Figure 2, respectively. The best fit of the magnetization as a function of the recovery time gives ^{13}C $T_1 = 0.86$ s for the 33 ppm peak and 0.26 s for the 31 ppm peak. Resonances from amorphous structures actually cover a range from about 29 to 33 ppm. It can be seen in Figure 2d that the ^{13}C T_1 is inhomogeneous for the amorphous peak centered at 31 ppm. These T_1 values increase with chemical shift, indicating the existence of fine structures for the amorphous region, in agreement with previously reported results.[11]

The dipolar dephasing time constant, T_{DD}, of the two slowly relaxing components in the peak located at 33 ppm was measured using the pulse sequence in Figure 1c. The magnetization was prepared before the usual dipolar dephasing period DD with a CP inversion−recovery segment employing a recovery time of $\tau = 0.3$ s so that the signal from the amorphous structures was suppressed and the signal from the fast relaxing component at 33 ppm was reduced by approximately 31%. The phase inverted spectrum with zero dephasing time is shown in Figure 2c, and the resultant time constant is $T_{DD} = 15 \pm 0.2$ μs.

The T_{DD} for the amorphous structure was obtained using the pulse sequence in Figure 1d, where a saturation−recovery ($d_1 = 0.4$ s) was employed before the dephasing period. The decay of the integral intensity as a function of the dephasing time is biexponential.[1,11] The parameters obtained from a best fit of the data give $T_{DD} = 30 \pm 1$ μs (65%, less mobile amorphous) and $T_{DD} = 1100 \pm 20$ μs (35%, mobile amorphous). Three selected spectra at dephasing times of 1, 20, and 900 μs are shown in Figure 3. It is found that the peak positions apparently are shifted from 31.17 ppm (1 μs) to 31.1 ppm (20 μs) to 31.03 ppm (900 μs), and the line width at half-height of the peaks are 155 Hz (1 μs), 139 Hz (20 μs), and 95 Hz (900 μs). This indicates that the resonance corresponding to the $T_{DD} = 30$ μs component is overlapped with that of the $T_{DD} = 1100$ μs component.

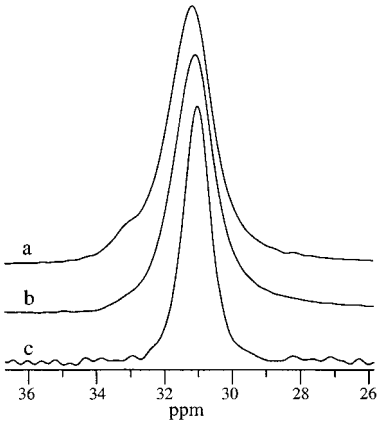

Figure 3. Spectra were obtained using the pulse sequence in Figure 1d at dephasing times of 1 (a), 20 (b), and 900 μs (c).

Table 1. NMR Parameters for the Four Types of Suggested Structures in PE[a]

component designation	LC	SC	LMA	MA
^{13}C T_1 (s)	1010 ± 10, 93 ± 5	0.86 ± 0.05	0.26 ± 0.02	0.26 ± 0.02
T_{DD} (μs)	15 ± 0.2	15.9 ± 0.5	30 ± 1	1100 ± 20
DCC (kHz)	22.8	~22.8	~10.5	~0−1.3
δ_{11} (ppm)	50.7	50	37.9	$\Delta\nu_{1/2}$ = 16
δ_{22} (ppm)	36.2	36	37.9	
δ_{33} (ppm)	12.2	12	18.5	
δ_{iso} (ppm)	33	33	31.5	31
%	59	9	21	11

[a] DCC = dipolar coupling constant. % = fraction of materials being part of that component. LC = crystalline structure with long ^{13}C T_1 values. SC = crystalline structure with short ^{13}C T_1 values. LMA = less mobile amorphous structure. MA = mobile amorphous structure. $\Delta\nu_{1/2}$ is the half-height width in ppm.

The T_{DD} for the short T_1 (0.86) component at 33 ppm was measured using the sequence in Figure 1e. A saturation−recovery delay (d_1 = 0.4 s) plus an inversion−recovery period (τ = 0.135 s) were employed prior to the variable dipolar dephasing period. The spectrum for DD = 0 μs is similar to that in Figure 2d. In this way the signal arising from the faster relaxing 33 ppm peak is emphasized while the signal from the amorphous structure is suppressed. The peak height of the 33 ppm peak as a function of dephasing time is fit by a single exponential with a dipolar dephasing time constant of T_{DD} = 15.9 ± 0.5 μs. This T_{DD} value is essentially the same, within the experimental error, as that of the resonance located at 33 ppm with long ^{13}C T_1 values (1010 and 93 s).

For convenience of discussion, we define four types of structures in PE (see Table 1). They are two types of crystalline structures abbreviated as LC and SC for long and short ^{13}C T_1 values, respectively, and two types of amorphous structures MA and LMA for mobile and less mobile structures, respectively.

2.2. 2D Separated-Local-Field (SLF) Experiments. The pulse sequences for the 2D separated-local-field (SLF) experiment and its saturation−recovery (SR) and saturation−recovery + dipolar dephasing (SRD) variations are given in Figure 4. Homonuclear dipolar decoupling using the flip-flop Lee Goldburg (FFLG) decoupling sequence[21−23] was employed during the dipolar evolution period.

The 2D SLF pattern given in Figure 5a contains all of the structures in the PE sample and may be obtained with the CP-SLF sequence in Figure 4a. The 2D SLF pattern in Figure 5b for the amorphous structures (LMA + MA) was obtained with the pulse sequence in Figure 4b. In this spectrum, the signal for the all-trans crystalline structures with ^{13}C T_1 = 1010 and 93 s (LC) was completely suppressed by a train of

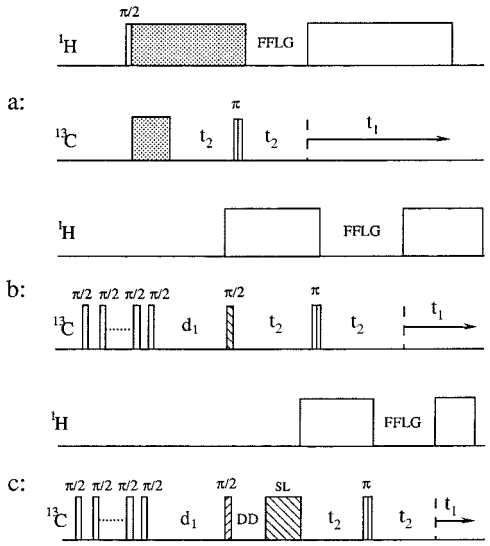

Figure 4. Pulse sequences for the 2D separated-local-field (SLF) experiments. (a) The cross-polarization SLF experiment, i.e., CP-SLF. (b) SLF combined with saturation−recovery, i.e., the SR-SLF. (c) SLF combined with saturation−recovery plus an additional dipolar dephasing period DD + SL, i.e., SRD-SLF, where the SL pulse is used to destroy the unwanted magnetization in the transverse plane which is perpendicular to the SL axis. Homonuclear dipolar decoupling using FFLG decoupling was employed during the dipolar evolution t_2 period.

saturation pulses separated by 200 μs. The signal for the ^{13}C T_1 = 0.86 s component (SC), though present, is of low intensity (see Figure 2b) and does not obscure the 2D SLF pattern in Figure 5b, which is a representation of the amorphous structure. The 2D SLF pattern shown in Figure 5c for the MA region was obtained using the pulse sequence in Figure 4c with a dipolar dephasing time of DD = 100 μs to eliminate completely the LMA structure.

To obtain the 2D SLF pattern for the SC structure, the pulse sequence in Figure 4b was again used with d_1 set to 4 s. This leaves the signal corresponding to the LC still satisfactorily saturated while the signals for the MA + LMA as well as SC are detected. The 2D SLF pattern for the SC structure is recognized though at a very low contour intensity. The resultant pattern for SC is emphasized in Figure 5d by plotting only the contour levels from 0.005 to 0.1 with an interval of 0.01.

2.3. ^{13}C Chemical Shift Tensor Principal Values at Room Temperature. The PHORMAT[18] experiment and its variations were performed on a Varian VXR-200 NMR spectrometer with a ^{13}C Larmor frequency of 50.309 MHz. A homemade MAT probe with a large sample volume of 6.0 cm^3, described previously,[17] was used for the room-temperature PHORMAT measurements. Two decoupling fields were employed: 30 kHz for cross-polarization and 48 kHz for decoupling.

The SR and SRD variations of PHORMAT sequences are depicted in Figure 6. In the SR-PHORMAT experiment (Figure 6a), the cross-polarization (CP) segment in the original PHORMAT sequence[18] is replaced by a π/2 pulse in the ^{13}C channel labeled "a". The phase of "a" is equal to the corresponding phase of the initial ^{1}H π/2 in the original PHORMAT sequence plus a 90° phase shift. The SRD-PHORMAT sequence is similar to that in Figure 6a, except for the addition of a dipolar dephasing segment, i.e., DD + SL. [17]

A conventional cross-polarization PHORMAT spectrum (CP-PHORMAT)[18] of the PE sample is shown in Figure 7a with the isotropic chemical shifts displayed along the evolution dimension (F_b) and the CSA tensor powder patterns along the acquisition dimension (F_a).

The 2D PHORMAT spectrum containing signals from the MA, LMA, and SC is given in Figure 7b. This spectrum used

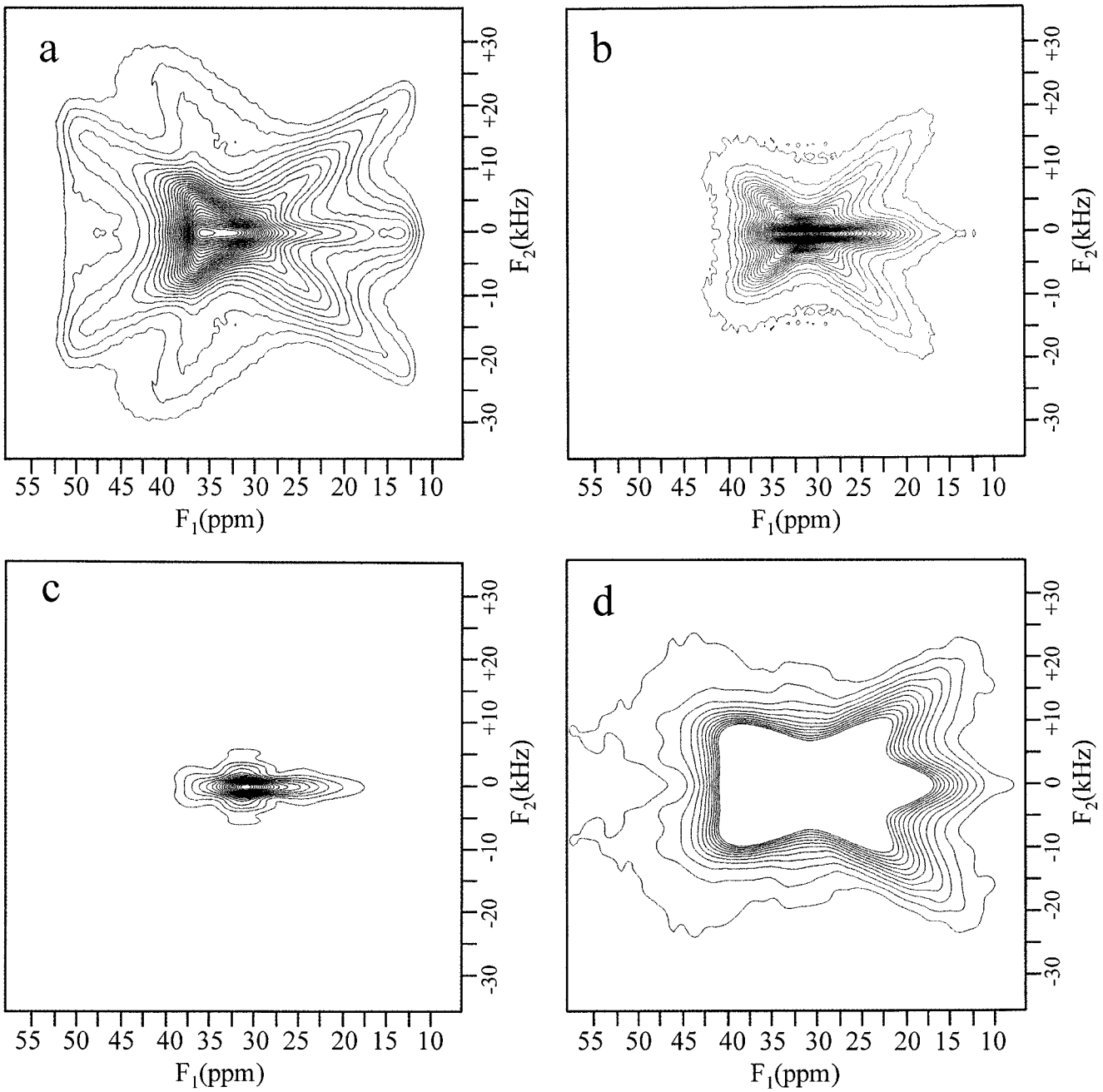

Figure 5. 2D SLF powder patterns of PE. (a) CP−SLF: flip-flop Lee−Goldburg (FFLG) homonuclear decoupling during the dipolar evolution dimension was applied. The ^{1}H decoupling field was 66.7 kHz, corresponding to a full FFLG cycle of 24.4 μs and a frequency offset of +47.14 kHz for the +LG and −47.14 kHz for the −LG, respectively. The experimentally determined scaling factor for the FFLG sequence is close to the theoretical value of 0.577. The dipolar evolution time t_2 was incremented by a full FFLG cycle time, i.e., 24.4 μs. Forty increments in the dipolar evolution dimension were acquired with a contact time of 1 ms, recycle delay time of 1 s, and 1024 scans for each increment. (b) SR-SLF: the experimental parameters are the same as those in (a), except d_1 = 0.4 and 2048 scans acquired for each dipolar evolution increment, t_2. (c) SRD-SLF: d_1 = 0.4 s and a dipolar dephasing period of DD = 100 μs. The rest of the experimental conditions are the same as those of (b), except 4000 scans were accumulated for each t_2 increment. (d) SR-SLF: d_1 = 4 s. The other experimental parameters were the same as those of (b).

the SR-PHORMAT sequence depicted in Figure 6a with a recovery time of d_1 = 2 s. The signal for MA and LMA is completely recovered along with about 90% of the SC signal. The intensity of the residual LC signal is less than 2% of its maximum intensity and may be ignored in Figure 7b.

The 2D SRD-PHORMAT pulse sequence in Figure 6b with a dipolar dephasing time of DD = 100 μs and a recovery time of d_1 = 0.4 s gives a spectrum of the MA, and the results are shown in Figure 7c.

By subtracting the appropriately weighted SR-PHORMAT spectrum in Figure 7b from that of Figure 7a to filter out the amorphous signal, one obtains a PHORMAT spectrum (Figure 7d) dominated by the LC. The residual SC signal in this difference spectrum is estimated to be less than 1.4%.

The projections onto the F_a and F_b axis for each of the 2D PHORMAT spectra in Figure 7 are given in Figure 8. The acquisition projection (F_a) resembles a stationary powder pattern because of the very low turning rate (i.e., 20 Hz) employed during the experiment. The evolution projection (F_b) resembles a high-resolution, high-speed MAS spectrum that is evident by comparing the top two right-hand traces in Figure 8 with their counterparts in Figure 2a,b.

The powder patterns sliced at several selected isotropic chemical shifts for each of the 2D spectrum in Figure 7 are summarized in Figure 9 for selected carbon nuclei.

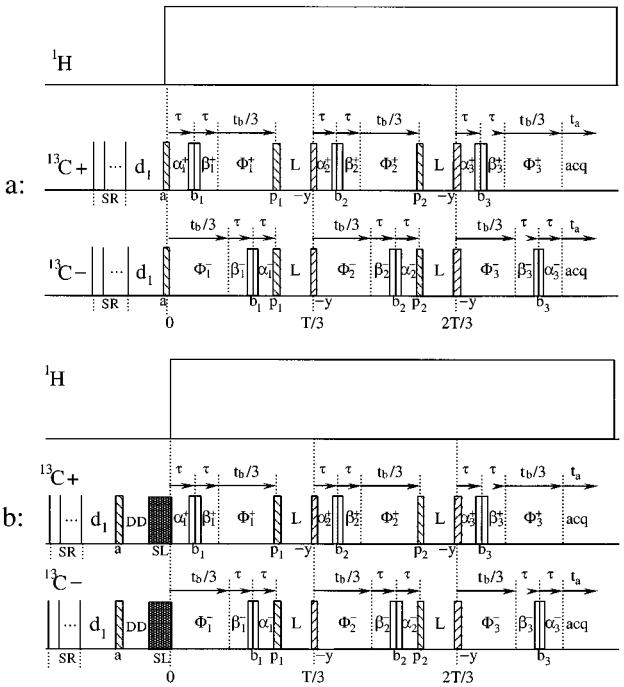

Figure 6. Pulse sequences for the anisotropic−isotropic 2D correlation spectrum by the PHORMAT method. (a) PHORMAT combined with saturation−recovery (d_1), i.e., the SR-PHORMAT. (b) PHORMAT combined with saturation−recovery (d_1) and dipolar dephasing (DD), i.e., the SRD-PHORMAT, where the phase of the SL pulse is $\pm x$.

3. Discussion

3.1. 2D Separated-Local-Field Experiment. The SLF patterns for the MA and LMA amorphous structure, Figure 5b,c, are concentrated in the central portion of the 2D SLF pattern given in Figure 5a. The overall butterfly pattern in Figure 5a is thus dominated by the all-trans LC structure.

Comparing the spectrum in Figure 5a with that in Figure 5d, it is found that the coupling patterns around the δ_{33} shift position (12.2 ppm) in Figure 5d are essentially the same as those in Figure 5a. The magnitude of the dipolar couplings near the δ_{11} (≈50 ppm) position is comparable to their counterpart in Figure 5a. Because the large intensity of the amorphous pattern is obscured in Figure 5d, it is difficult to recognize the low-intensity features (around 40−50 ppm). Since the dipolar dephasing constants ($T_{DD} \approx 15$ μs) are similar for both the LC and SC structures, the 2D SLF patterns for both the SC and LC in PE are believed to be essentially the same. This result indicates that the principal values of the chemical shift tensors along with their orientations in the molecular frame are similar for both structures (see Table 1), and thus, the local electronic environments of LC and SC are similar.

As the dipolar interaction is the dominant mechanism for ^{13}C relaxation in most organic solids, the effective molecular motion can be expected to average the dipolar interaction between ^{13}C and ^{1}H spins as well as the ^{13}C chemical shift anisotropy (CSA). The span of the CSA at 4.7 T field ($(\delta_{33} - \delta_{11}) \times \upsilon_0 \times 10^{-6}$ Hz ≈ 1900 Hz) is much smaller than the ^{13}C−^{1}H dipolar coupling constant (i.e., about 22.8 kHz in PE). Hence, effective molecular motion with a frequency faster than 1900 Hz does not exist for the SC structure. This result strongly supports the previous suggestion based on a 2D exchange experiment[13] that chain diffusion between the amorphous and the crystalline region in polyethylene is the basic reason for the nonexponential ^{13}C T_1 observed for the crystalline component of PE. The short ^{13}C T_1 value of 0.86 s for SC structure results from chains that have diffused from the amorphous region into the crystalline lamellar region. The short ^{13}C T_1 value may be explained if the magnetization transferring time between the LMA and the SC conformations is shorter than, or comparable to, the relaxation time constant of the LMA conformations. Once the chain diffuses into the lattice of the crystalline region, they become relatively rigid on the NMR time scale because of the restricted motion due to the surroundings and thus are characterized as crystalline. The predicted diffusion rate (or the jump rate) at room temperature that can obtained by using the data from ref 13 is indeed much less than 1900 Hz, a condition required to preserve both the dipolar coupling and the CSA tensor. Since the time required for the magnetization transfer from LMA to LC region should be related to both the chain jump rate and the carbon locations in these two regions, a distribution of ^{13}C T_1 would follow.

This result varies from a previous report where the crystalline structure with a short ^{13}C T_1 (1−3 s) at 33 ppm in PE has been interpreted as an intermediate structure (i.e., the less mobile amorphous structure).[14] However, because the crystalline structure with a short ^{13}C T_1 constantly exchanges with the less mobile amorphous structure through chain diffusion, an equilibrium state may be reached between these two types of structures. In other words, the fraction of the less mobile amorphous structure may be proportional to that of the crystal structure with short ^{13}C T_1 value. Consequently, the discussions[14] regarding the interfacial structures based on the percentage of the crystalline structure with short ^{13}C T_1 values may still be relevant with these new interpretations applied.

As the orientation of the shift principal values with respect to the ^{13}C−^{1}H dipolar bond direction may be determined by the 2D SLF powder pattern of the corresponding shift tensor, this geometrical information may be extracted readily at the δ_{11}, δ_{22}, and δ_{33} positions. The Hamiltonian establishes this relationship in accordance with the following equation.

$$H = \sum A_j S_z I_{zj}, \quad j = 1, 2$$
$$A_j(\theta) = D_j(3\cos^2(\theta_j) - 1) \qquad (1)$$
$$D_j = \gamma_I \gamma_S / r_j^3$$

where θ_j is the angle between the C−H$_j$ vector and the B_0 direction for the jth bonded proton. When the magnetic field lies along the δ_{33}, i.e., parallel to the all-trans chain direction, $\theta_j = 90°$ for both $j = 1$ and 2, the coupling pattern at δ_{33} will be a triplet with a separation between the adjacent peaks equal to D_j. This triplet pattern is clearly observed for the B_0 along the δ_{33} position (see Figure 5a) with a dipolar coupling constant of about 22.8 kHz, corresponding to a CH distance of 1.095 Å. These results confirm the early finding that the δ_{33} component is along the chain direction.[24] It is observed from Figure 5a that the dipolar pattern is considerably reduced at the frequency of the δ_{22} component of the shift tensor. Note that δ_{22} lies at the bisector of the two C−H bond vectors separated by the tetrahedral angle. One-half of a near tetrahedral angle

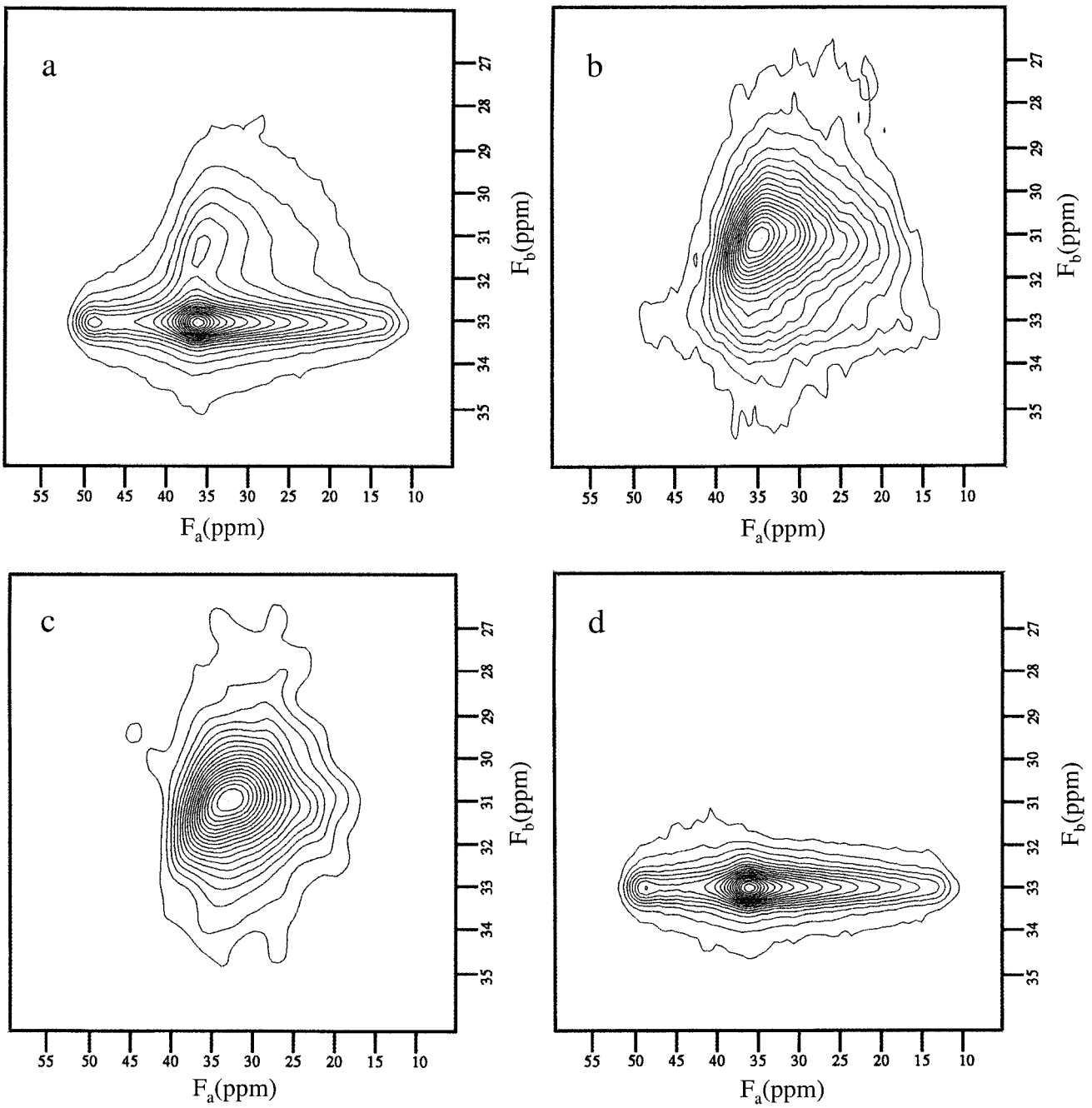

Figure 7. (a) CP-PHORMAT: A sample turning frequency of 20 ± 0.2 Hz was used. The cross-polarization contact time was 1 ms, and the echo time τ was 50 μs. The recycle delay time was 2 s. Acquisition dimension (t_a) FIDs with 640 complex points were transformed to spectra with a 40 kHz spectral width. The 2D PHORMAT data were collected at 33 t_b values incremented by periods of 1 ms. This results in a maximum evolution time of 33 ms and an evolution-dimension spectral width of 1 kHz. The eight types of free-induction decay[18] were acquired with the (+) and (−) PHORMAT pulse sequences using a total of 1000 scans at each t_b value, resulting in a total measuring time of about 19 h. (b) SR-PHORMAT: The spectrum was acquired using the same experimental conditions as those of Figure 7a except only 20 t_b values were acquired and a measuring time of about 12 h was used. (c) SRD-PHORMAT: The rest of the experimental parameters are the same as those of (b) except 17 t_b increments and 4000 scans for each t_b were acquired. The experimental time was about 38 h. (d) (a)−k*(b), where k is adjusted so that the difference spectrum contains minimum signal from amorphous structures.

gives the magic angle that reduces A_j in eq 1 to either a zero or negligible value, again confirming the previous result[24] that δ_{22} bisects the H−C−H angle. The remaining δ_{11} component, by default, must then orient parallel to the inter-proton−proton vector.

The 2D SLF pattern in Figure 5b is a superposition of 2D SLF patterns for both the LMA and MA structures. Subtracting the 2D SLF pattern for the MA pattern given in Figure 5c, one obtains the 2D SLF pattern for the LMA component. As the dipolar coupling constant for the LMA component found at δ_{11} (38 ppm) is approximately $^1/_2$ of the dipolar coupling constant of the all-trans LC and SC structures, it is clear that molecular motion is partially averaging the dipolar couplings. This also explains why the dipolar dephasing constant $T_{DD} = 30$ μs for LMA is 2 times that (15 μs) of the all-trans LC and SC structures centered at 33 ppm. Types of molecular motion in the amorphous regions of linear polyethylene have been investigated previously by Spiess' group using deuteron NMR.[25,26] In the fol-

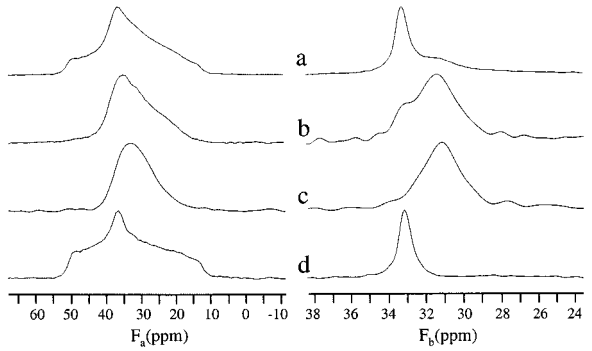

Figure 8. Projections of Figure 7 onto the F_a (left) and F_b (right) axes. (a) CP-PHORMAT, (b) SR−PHORMAT, (c) SRD-PHORMAT, and (d) (a)−k*(b). *K* is a constant which is determined so that the amorphous signal is minimized in the difference spectrum.

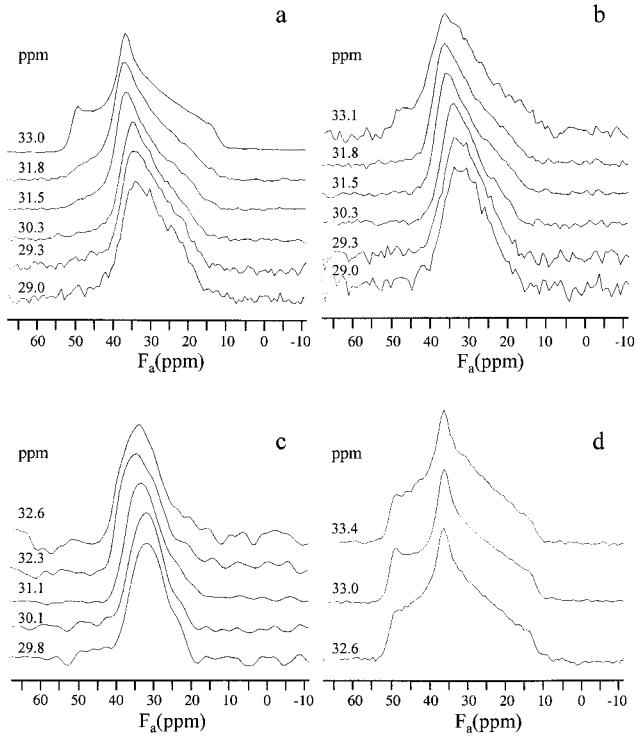

Figure 9. Powder patterns sliced at several selected isotropic chemical shifts for each of the 2D spectrum in Figure 7. (a) CP-PHORMAT, (b) SR-PHORMAT, (c) SRD-PHORMAT, and (d) (a)−k*(b).

lowing, a simplified motional model is proposed to explain the SLF powder pattern for the LMA structures.

In general, if a CH_2 group is rotated about an axis inclined at an angle θ with respect to the external magnetic field direction at a rate that is larger than the width of the dipolar coupling, the effective dipole−dipole interaction Hamiltonian for the system is reduced. This is given by[27]

$$H = \sum A_j S_z I_{zj}, \quad j = 1, 2$$

$$A_j(\beta,\theta) = D_j((^3/_2)\sin^2(\beta_j) - 1)(1 - 3\cos^2(\theta)) \quad (2)$$

$$D_j = \gamma_I\gamma_S/r_j^3$$

where β_j is the angle between the rotation axis and the C−H_j vector direction for the *j*th bonded proton, $j = 1$, 2 for a CH_2 group. A reduction of dipolar coupling constant allows β to be calculated from the $((^3/_2)\sin^2(\beta_j) - 1)$ term. This gives $\beta_j = 90°$ for $j = 1$ and 2. To satisfy $\beta_j = 90°$ for the δ_{11} and δ_{22} components at 38 ppm, the chain segment must rotate about the long chain axis in the all-trans conformations of the LMA structure. This conclusion is both intuitive and reasonable. However, it should be pointed out that the rotation about the trans axis is a tentative conclusion since the $^1/_2$ reduction in the dipolar coupling is only approximate (see Table 1).

From Figure 5c it may be concluded that the dipolar coupling between C−H is averaged further by molecular motion in the MA structure, indicating that the molecular motion in the MA structure approaches isotropic tumbling because some residual CSA is still observed that will be detailed.

3.2. ^{13}C Chemical Shift Tensor. The crystallinity of the PE sample is defined as the ratio of the all-trans crystal structure centered about 33 ppm (see Figure 7d) to the total integral of the band given in Figure 7a. The resulting 76% value is qualitatively in agreement with that (68 ± 1%) obtained from a single-pulse (SP) experiment (not shown) using a recycle delay time of 3500 s. Such a discrepancy between CP and SP crystallinities is well-known because the ^{13}C−^{1}H dipolar coupling in the amorphous structures is greatly reduced even on a static sample (see Figure 5c). In Table 1, only the crystallinity from SP is reported. The fraction of the LMA structure (21%) may be deduced from the relative fraction of amorphous signal with the remaining 11% attributed to the MA structure.

Upon examining the powder spectral slices (Figure 9a) at incrementally increased isotropic chemical shifts of the CP-PHORMAT spectrum in Figure 7a, one clearly observes the changes and transitions of the powder patterns from motionally narrowed amorphous structures to the rigid crystal structures. Furthermore, the spectral analysis is complicated by the existence of four kinds of structures in PE. The superposition of their powder patterns in the overlapped CP-PHORMAT spectrum also increases the difficulty of interpretation. This complexity in Figure 9a is simplified by the SR-PHORMAT (Figures 7b and 9b), the SRD-PHORMAT (Figures 7c and 9c), and the difference spectra (Figures 7d and 9d).

The difference spectrum, given in Figure 7d, represents the 2D PHORMAT pattern for the LC all-trans crystal structure. The powder pattern slice at 33 ppm, plotted in Figure 9d, is essentially the same trace as that in Figure 9a from the CP-PHORMAT spectrum, indicating that a simple structural type is found at this shift value. These two powder pattern slices are slightly distorted because of insufficient ^{1}H decoupling, i.e., about 48 kHz, in this experiment. Strong dipolar coupling may be observed at these corresponding chemical shift ranges for the 2D SLF result shown in Figure 5a. By projecting all the data in Figure 7d onto the F_a axis, the distortion disappears as expected, and the result is given at the bottom left of Figure 8. This spectrum may be simulated with a single tensor. The resultant principal values, corresponding to the LC all-trans crystal structure, are given in Table 1 with $\delta_{11} =$ 50.7 ppm, $\delta_{22} = 36.2$ ppm, and $\delta_{33} = 12.2$ ppm.

The shape of the powder slices for the MA structures is dominated by a prominent Gaussian line shape (Figure 9c). The pattern, which is shifted downfield with an increase in isotropic chemical shift values, exhibits widths (about 16 ppm) that are still much larger than

the approximately 4 ppm isotropic chemical shift range of the mobile amorphous structure (see Figures 2 and 3 and Figure 9c). The motions involved in the mobile amorphous structure approach isotropic tumbling, but some constrained reorientational motion remains. The downfield shift of the powder pattern with increasing isotropic chemical shift value indicates a diversity of molecular conformations in the MA structure. Since the mobile amorphous molecular segments should involve a variety of gauche conformations, these results also suggest a variety of dynamic structures and chain lengths for the mobile moieties.

The ^{13}C CSA principal values for the SC all-trans structure can be easily identified by examining the powder patterns at the 33 ppm isotropic chemical shift values in Figure 7b. A typical slice is shown as the top trace in Figure 9b. Though this slice still exhibits with some of the amorphous tensors, the prominent break points of the shift tensor corresponding to the SC can be easily identified. The resultant ^{13}C principal values are $\delta_{11} = 50$ ppm, $\delta_{22} = 36$ ppm and $\delta_{33} = 12$ ppm.

One can also identify the ^{13}C principal values for the LMA structure by comparing the spectral slices in parts a−c of Figure 9. The results are approximately $\delta_{11} = \delta_{22} = 37.9$ ppm and $\delta_{33} = 18.5$ ppm, which were obtained from the spectral slice at 31.5 ppm in Figure 9b.

The chemical shift component δ_{zz} along a magnetic field direction $\mathbf{B}_0$, designated as the z-axis in the laboratory frame, is related to the principal values of the chemical shift tensor by[1]

$$\delta_{zz} = \delta_{11}^0 \sin^2\beta_0 \cos^2\gamma_0 + \delta_{22}^0 \sin^2\beta_0 \sin^2\gamma_0 + \delta_{33}^0 \cos^2\beta_0 \quad (3)$$

where β_0 is the polar angle between $\mathbf{B}_0$ and the δ_{33}^0 principal axis and γ_0 is the azimuthal angle of rotation about the δ_{33}^0 axis. The principal values of the tensor without motional averaging are δ_{11}^0, δ_{22}^0, and δ_{33}^0. The SLF experiments indicate that the LMA structure prefers the trans conformation, and rotation occurs primarily about the trans chain axis (i.e., the δ_{33}^0) at a rate larger than the width of the shift tensor. Under the assumption of a single rotation about the trans chain axis, eq 3 becomes

$$\delta_{zz} = {}^1/_2(\delta_{11}^0 + \delta_{22}^0) \sin^2\beta_0 + \delta_{33}^0 \cos^2\beta_0 \quad (4)$$

where average of both $\cos^2\gamma_0$ and $\sin^2\gamma_0$ for a circular motion about the trans axis is $^1/_2$. Equation 4 describes an axially symmetric CSA tensor. The value of the effective component perpendicular to the rotation axis is $\delta_\perp = {}^1/_2(\delta_{11}^0 + \delta_{22}^0)$, while the component parallel to the rotation axis remains $\delta_\parallel = \delta_{33}^0$. To verify the relationship (eq 4) between the values of $\delta_\perp$ and $\delta_\parallel$, and the values of δ_{11}^0, δ_{22}^0, and δ_{33}^0, both sets must be determined.

We have performed CP-PHORMAT experiments at a temperature of −118 °C. The data indicate an increase in crystallinity, consistent with results drawn from deuterium NMR studies.[25,26] However, the shape of the tensor for the amorphous structures at an isotropic chemical shift value of around 31.5 ppm is not changed compared to that in Figures 7a and 9a. This result indicates that the increase of crystallinity is associated with conformational change in the amorphous structure of PE; i.e., some of the gauche structures convert to trans structures, and some trans structures associated with LMA at room temperature become ordered rigid trans structures. Consequently, the isotropic chemical shift value of these LMA structures moves into the 33 ppm peak. We, therefore, tentatively assign the corresponding principal values of the LC or SC to δ_{11}^0 (50.7), δ_{22}^0 (36.2), and δ_{33}^0 (12.2).

A simple uniaxial model of rotation about the trans axis would give values of 43.5 and 12.2 ppm for $\delta_\perp$ and $\delta_\parallel$, respectively. But the actual experimental principal values for the LMA are $\delta_{11} = \delta_{22} = 37.9$ ppm and $\delta_{33} = 18.5$ ppm (Table 1). The averaged experimental values deviate by approximately 6 ppm from the idealized case of rotation about the single trans axis. This result suggests some further motional averaging. Translational diffusion along the direction of the chain axis, though it likely exists, would not be expected to affect the observed CSA tensor. Conversely, librations of the chain about axes other than the chain axis would further average the CSA tensor from the idealized single rotation along the trans axis. Such motions would account for the observed LMA tensor. Motions associated with changes between trans and gauche conformations due to serpentine diffusional motion of the LMA structure also could affect these results. Since the isotropic chemical shift value is insensitive to rotational averaging, assigning the principal values of LC (or SC) to the δ_{11}^0, δ_{22}^0, and δ_{33}^0 therefore have relatively minor discrepancies because the isotropic chemical shift values for LC and LMA structures differ only by about 1.5 ppm. Unfortunately, the exact δ_{11}^0, δ_{22}^0, and δ_{33}^0 for the LMA are presently unavailable, and it is not possible to discuss the minor differences from those in the LC (or SC) structures.

4. Conclusions

Four types of suggested structures have been investigated in polyethylene, i.e., two types of crystalline structures (LC and SC) and two types of amorphous structures, the less mobile amorphous (LMA) and mobile amorphous (MA). Both LC and SC crystalline structures have essentially the same isotropic chemical shift value but differ distinctly in ^{13}C spin−lattice relaxation times. The dipolar dephasing time constants, the 2D SLF powder patterns, and the principal values of the ^{13}C CSA are all essentially the same for both the LC and SC crystalline structures. These results strongly support the previous suggestion[12,13] that chain diffusion between the amorphous region and the crystalline region of the polymer is the primary reason for the multiple-exponential ^{13}C T_1 decay found in the crystalline structure in PE.

The LMA and MA structures are clearly distinguishable by their distinct dipolar dephasing time constants. The LMA structure in PE adopts preferably the trans conformation, and the trans segment rotates dominantly about the trans chain axis at a rate larger than the width of the dipolar coupling in a rigid CH_2 group. As a result, the dipolar coupling constant is reduced to approximately one-half of its nonaveraged value while the CSA tensor is averaged to an effective axial symmetric tensor. Segmental motion involved in the MA structure approaches isotropic tumbling. However, the motion is not isotropic because the chemical shift tensor is not completely averaged to its isotropic value.

Acknowledgment. The authors are grateful to Drs. D. W. Alderman, Mark S. Solum, and Anita M. Orendt

for their many helpful discussions. This work was supported by the Office of Basic Energy Science of DOE under Grant DE FG02-94 ER 14452, by the NIH under GM 08521-38, and by Pittsburgh Technology Center (PETC) by a contract to the Consortium for Fossil Fuel Liquification Science. Dr. Jian Zhi Hu was supported partially by a Fellowship from the Green Chemistry Program of Los Alamos National Laboratory through the Associated Western Universities.

References and Notes

(1) McBrierty, V. J.; Packer, K. J. *Nuclear Magnetic Resonance in Solid Polymers*; Cambridge University Press: Cambridge, 1993.
(2) Fujimoto, K.; Nishi, T.; Kado, R. *Polym. J*. **1972**, *3*, 448.
(3) Bergmann, K. *Polym. Bull*. **1981**, *5*, 355.
(4) McBrierty, V. J.; Douglass, D. C.; Barham, P. J. *J. Polym. Sci., Polym. Phys. Ed*. **1980**, *18*, 1561.
(5) Doskocilova, D.; Schneider, B.; Jakes, J.; Schmidt, P.; Baldrian, J.; Hernandez- Fuentes, I.; Caceres Alonso, M. *Polymer* **1986**, *27*, 1658.
(6) Cheung, T. T. P.; Gerstein, B. C. *J. Appl. Phys*. **1981**, *52*, 5517.
(7) Pembleton, R. G.; Wilson, R. C.; Gerstein, B. C. *J. Chem. Phys*. **1977**, *66*, 5133.
(8) Earl, W. L.; VanderHart, D. L. *Macromolecules* **1979**, *12*, 762.
(9) Cudby, M. E. A.; Packer, K. J.; Hendra, P. J. *Polym. Commun*. **1984**, *25*, 303.
(10) Colquhoun, I. J.; Packer, K. J. *Br. Polym. J*. **1987**, *19*, 151.
(11) Kitamaru, R.; Horii, F.; Murayama, K. *Macromolecules* **1986**, *19*, 636.
(12) VanderHart, D. L. *J. Magn. Reson*. **1987**, *72*, 13.
(13) Schmidt-Rohr, K.; Spiess, H. W. *Macromolecules* **1991**, *24*, 5288.
(14) Cheng, J.; Fone, M.; Reddy, V. N.; Schwartz, K. B.; Fisher, H. P.; Wunderlich, B. *J. Polym. Sci., Part B: Polym. Phys*. **1994**, *32*, 2683.
(15) Torchia, D. A. *J. Magn. Reson*. **1978**, *30*, 613.
(16) Gan, Z. *J. Am. Chem. Soc*. **1992**, *114*, 8307.
(17) (a) Hu, J. Z.; Alderman, D. W.; Ye, C.; Pugmire, R. J.; Grant, D. M. *J. Magn. Reson., Ser. A* **1993**, *105*, 82. (b) Hu, J. Z.; Orendt, A. M.; Alderman, D. W.; Pugmire, R. J.; Ye, C.; Grant, D. M. *Solid State NMR* **1994**, *3*, 181.
(18) Hu, J. Z.; Wang, W.; Liu, F.; Solum, M. S.; Alderman, D. W.; Pugmire, R. J.; Grant, D. M. *J. Magn. Reson., Ser. A* **1995**, *113*, 210.
(19) Gan, Z.; Ernst, R. R. *J. Magn. Reson., Ser. A* **1996**, *123*, 140.
(20) Linder, M.; Hohener, A.; Ernst, R. R. *J. Chem. Phys*. **1980**, *73*, 4959.
(21) Bielecki, A.; Kolbert, A. C.; Levitt, M. H. *Chem. Phys. Lett*. **1989**, *155*, 341.
(22) Bielecki, A.; Kolbert, A. C.; DE Groot, H. J. M.; Griffin, R. G.; Levitt, M. H. *Adv. Magn. Reson*. **1990**, *14*, 111.
(23) Lee, M.; Goldburg, W. I. *Phys. Rev*. **1965**, *140*, A1261.
(24) Vanderhart, D. L. *J. Chem. Phys*. **1976**, *64*, 830.
(25) Hentschel, D.; Sillescu, H.; Spiess, H. W. *Polymer* **1984**, *25*, 1078.
(26) Spiess, H. W. *Colloid Polym. Sci*. **1983**, *261*, 193.
(27) Hu, J. Z.; Alderman, D. W.; Pugmire, R. J.; Grant, D. M. *J. Magn. Reson*. **1997**, *126*, 120.

MA9916842